# *Nonlinear Analysis of Nathpa Jhakri Powerhouse Cavern - A Case Study*

***Moataz A. Al-Obaydi*,***
***N. K. Samadhiya*****
***&***
***M. N. Viladkar*****

*Department of Civil Engineering,
College of Engineering,
University of Mosul, Mosul, Iraq

**, ***Department of Civil Engineering
Indian Institute of Technology, Roorkee- 247 667, India
**Email : nksamfce@iitr.ernet.in
***Email : sumanfce@iitr.ernet.in

0

**ABSTRACT**

Nathpa-Jhakri hydro-power project has been constructed in lesser Himalaya in the northern state of Himachal Pradesh in India. The project site is characterized by a very rugged topography with lofty hills. An underground power house with an installed capacity of 1500 MW of this project is considered to be the largest power house in a single cavern in India. In the present study, an attempt has been made to carry out a three dimensional finite element analysis for prediction of stresses and deformations around the powerhouse cavern.

In the present study, a 2-D model proposed by Sharma et al. (2001) to simulate the sequence of excavation has been extended to the case of actual three dimensional nature of excavation and the model proposed by Bandis et al. (1983) and Wang et al. (2003) for joint nonlinearity has also been incorporated. Results thus prove the capability of the software package developed for analyzing the stability of underground structures excavated in varying and complex geological settings. The type and the number of stages selected for simulation of excavation significantly influence the redistribution of stresses and, in turn, the stability of underground structures. An interesting observation made in this study is that it is not essential that the final stage of excavation is critical point of view of stability. Instead, the instability may occur at any intermediate stage of excavation. The critical stage of excavation along with an identical pattern of excavation can be detected by the proposed 3D-excavtion process.

***Keywords:*** Rock mass; Finite element method; Modeling; Stage-wise excavation; Underground opening

## 1. INTRODUCTION

Large underground facilities are being used for various purposes and a rapid growth in its utilization has taken place during the last few decades. Underground structures are often constructed in complex geological media which consist of jointed rock mass intersected by many discontinuities such as joints, faults, shear zones etc. All these discontinuities play an important role in governing the behavior of rock mass and in turn, the stability of underground structures and therefore the influence of such discontinuities must be included in the analysis.

The pattern of excavation, i.e. the excavation process and its sequence has a pronounced effect on the deformations and stress redistribution (Ranadive and Parikh, 2003). Numerical methods have been employed by various authors to evaluate the traction force on the excavated surface. Finite element method was used by Clough and Woodward (1967) to simulate the excavation process. Algorithms proposed by Christian and Wong (1973), Clough and Mana, 1976; and Mana and Clough, 1981 were found to violate the requirement uniqueness. Desai and Sargand (1984) succeeded in achieving the uniqueness of the solution by employing a hybrid method. Najjar and Zaman (1993) adopted an incremental-iterative solution algorithm based on whether a particular element is active or not, i.e. its location with respect to the excavated area.

Sharma et al. (1985) proposed another method for simulation of excavation in which the excavated elements were replaced by 'air' elements to satisfy the uniqueness requirements. The method was applied using elasto-plastic finite element analysis of a multi-stage excavation process and employing Mohr-Coulomb and Drucker-Prager failure criteria.

Another approach that has been adopted is to reduce the stiffness of excavated elements to an infinitesimally small value (Borja et al., 1989) so as to overcome the uniqueness problems. Comodromos et al. (1993) presented a static condensation method to overcome the numerical instability due to removal of elements and nodes. Sharma et al. (2001) omitted the excavated elements and nodes from the assembly of equations. This satisfied the uniqueness requirements.

In the present study, Nathpa-Jhakri powerhouse cavern has been selected to check the validity of the methodology proposed for three dimensional simulation of sequence of excavation.

## 2. POWERHOUSE CAVERN

In India, many hydropower projects are either in planning or design or construction stages for utilizing the maximum untapped hydropower potential. Many factors such as geological conditions, hydrology and economics are taken into consideration in planning and design of these projects. Nathpa-Jhakri Project is one such project in the state of Himachal Pradesh located in lesser Himalaya. The underground powerhouse cavern of this project, which is the largest cavern in the country, is located on the left bank of river Satluj at Jhakri. The powerhouse complex consists of two parallel caverns,

the machine hall cavern is 20 m wide, 49 m high and 216 m long and accommodates 6 units of 250 MW each whereas the transformer hall cavern is 17.5 m wide, 27.4 m high and 196 m long. The machine and transformer halls are separated by a 63 m wide rock pillar (Gupta, 1999).

The machine hall cavern is oriented in the North-South direction in such a manner that none of the shear planes runs parallel to the longitudinal axis of the cavern. The rock cover above the cavern is roughly about 300 m (Sharma and Chauhan, 1999).

## 3. STAGES OF EXCAVATION OF POWERHOUSE CAVERN

In the present study**,** the machine hall cavern has been considered for analysis. The cavern has been analyzed as a two-dimensional problem by various other investigators considering different stages of excavation ranging from three stages (Bhasin et al., 1995; and Chryssanthakis et al., 1996) to 12-stages (Sitharam and Latha, 2002). Varying excavation stages have been reported and adopted by other investigators also (Dasgupta, 1998; Chauhan, 1999; Sharma and Chauhan, 1999; and Sirkek et al., 1999).

In the present study, twenty seven stages of the bench excavation, including three stages in every heading and comprising of nine such headings, have been adopted for the three-dimensional analysis in the manner shown in Fig. 1. It may not be very much identical to the actual field excavation process sequence, though however, such a large number of excavation stages are considered to be a very good representation of the excavation sequence.

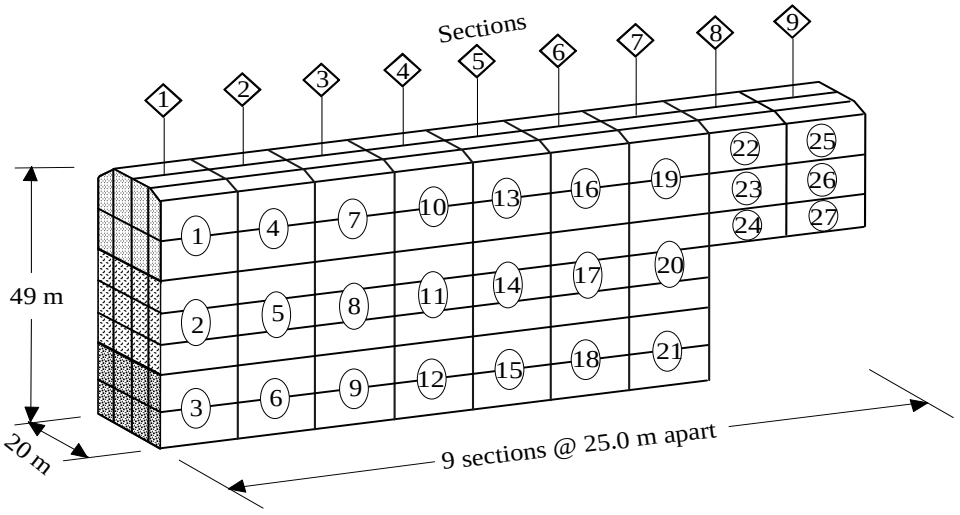


Fig. 1 - Sequences of excavation followed in present study

## 4. JOINT ORIENTATION IN ROCK MASS

The rock joints in the Nathpa-Jhakri area are irregular in nature and about five joint sets have been identified in the project area. Three major sets of joints have been identified

by Chryssanthakis et al. (1996) as critical joint sets which may affect the stability of the cavern. Joint set-I is a foliation joint which strikes in the East-West direction across the long axis of the cavern and dipping at $35^o$ towards the north. Other two joint sets (set-II and set-III) strike approximately in the North-South direction and are steeply dipping ($70^o$ – $90^o$) in the East and West directions respectively. Joint set-I is considered to be responsible affecting the stability of cavern due to the presence of gouge in it. Some shear zones have also been found whose trends are similar to the foliation joints and have thickness ranging from 10-20 cm.

In the present study, these three joint sets have been considered in all the analyses. The stereographic projection of the joint sets has been presented in Fig. 2. No shear zones have been considered in the present study.

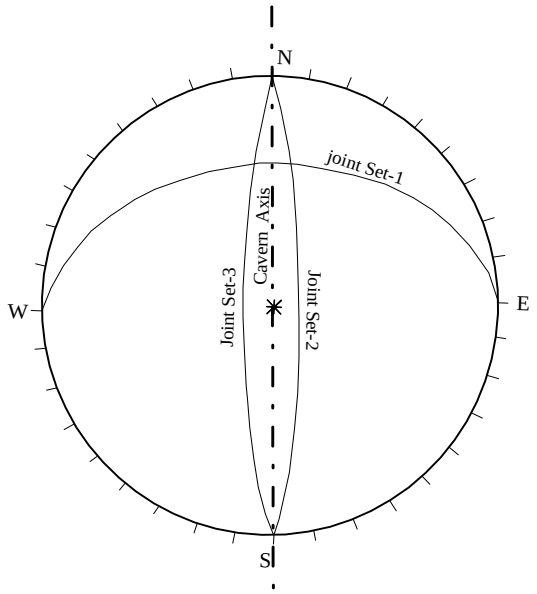


Fig. 2 - Stereographic projection of the joint sets

## 5. FIELD INSTRUMENTATION

The geological investigation, field measurements and analysis were carried out simultaneously during the construction of the Nathpa-Jhakri Project in order to check the stability of various structures. Field instrumentation programme was executed by installing Multiple Point Borehole Extensometers (MPBX) on the roof of the pilot tunnel and sidewalls of the cavern at different sections to monitor the deformations in rock mass (Bhasin et al., 1995). Figure 3 shows the locations and distribution of MPBXs around the cavern (Bhasin et al., 1996).

Table 1 gives details of excavation levels at the time of installation of MPBXs and the locations at specified sections and have been presented in Fig. 4 (Sitharam and Latha, 2002). Measured displacements have been compared with the predicted ones through numerical analysis.

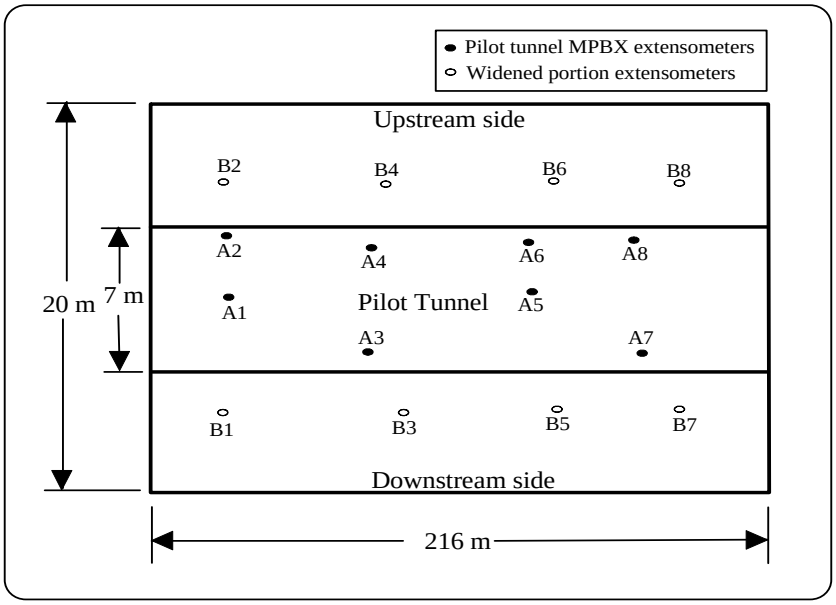


Fig. 3 - Plan of location of the instruments along the cavern
(Bhasin et al., 1996)

Table 1 – Location of MPBXs with respect to the excavation stage in cavern
(Sitharam and Latha, 2002)

| Location of Instruments | Instruments Installed at Elevation (m) | Elevation of Excavation Level When the MPBXs were Installed (m) |
|---|---|---|
| A | 1024 | After the excavation of drift |
| B | 1022 | 1018 |
| C | 1022 | 1006 |
| D | 1006 | 1000 |
| E | 996 | 983 |

## 6. MATERIAL PROPERTIES

Table 2 gives the properties of rock joints and the rock material. The behavior of joints has been represented by the normal and tangential stiffnesses of the joint sets.

## 7. LOADINGS

In-situ stresses as well as uniformly distributed load on the top boundary of domain have been considered in the present analysis. An overburden of 262.5 m has been considered by applying a distributed load of 4.792 MPa on the top boundary.

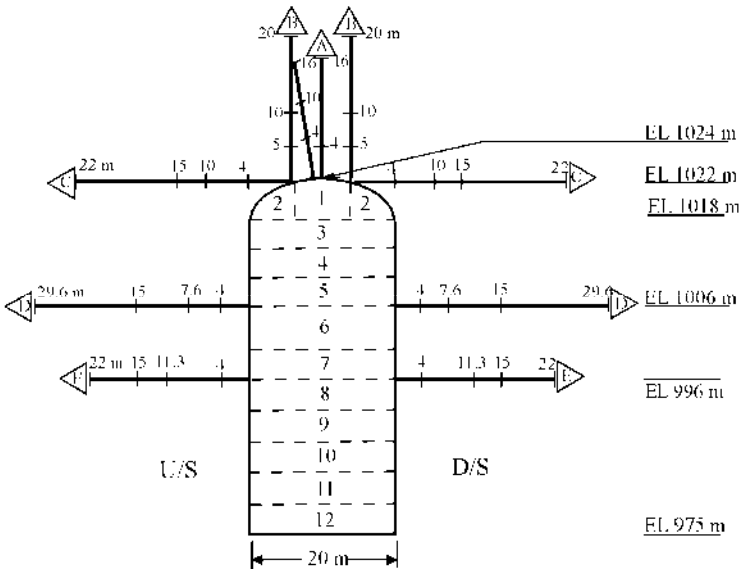


Fig. 4 - Location of MPBXs at the periphery of cavern
(Sitharam and Latha, 2002)

Table 2 - Material Properties (Bhasin et al., 1995)

| Material Type | S. No. | Material Properties | Symbol | Unit | Value |
|---|---|---|---|---|---|
| Rock Material | 1 | Modulus of elasticity | E | MPa | 13000 |
| | 2 | Poisson's ratio | $\nu$ | - | 0.20 |
| | 3 | Unit weight* | $\gamma$ | kN/m$^3$ | 27.0 |
| | 4 | Coefficient of lateral earth pressure at rest | $k_o$ | -- | 0.62 |
| Joint Set-I | 6 | Normal stiffness* | $k_n$ | MPa/m | 130000 |
| | 7 | Shear stiffness* | $k_s$ | MPa/m | 13000 |
| | 8 | Initial mechanical aperture | $E_0$ | mm | 0.17 |
| | 9 | Joint spacing | $S$ | m | 0.19 |
| | 10 | Dip | $\psi_j$ | Deg. | 35 |
| | 11 | Dip direction | $\alpha_j$ | Deg. | 0 |
| | 12 | Joint roughness coefficient | $JRC$ | - | 10 |
| Joint Set-II | 13 | Normal stiffness* | $k_n$ | MPa/m | 130000 |
| | 14 | Shear stiffness* | $k_s$ | MPa/m | 13000 |
| | 15 | Initial mechanical aperture | $E_0$ | mm | 0.19 |
| | 16 | Joint spacing | $S$ | m | 0.19 |
| | 17 | Dip | $\psi_j$ | Deg. | 80 |
| | 18 | Dip direction | $\alpha_j$ | Deg. | 90 |
| | 19 | Joint roughness coefficient | $JRC$ | - | 11 |
| Joint Set-III | 20 | Normal stiffness* | $k_n$ | MPa/m | 130000 |
| | 21 | Shear stiffness* | $k_s$ | MPa/m | 13000 |
| | 22 | Initial mechanical aperture | $E_0$ | mm | 0.19 |
| | 23 | Joint spacing | $S$ | m | 0.19 |
| | 24 | Dip | $\psi_j$ | Deg. | 80 |
| | 25 | Dip direction | $\alpha_j$ | Deg. | 270 |
| | 26 | Joint roughness coefficient | $JRC$ | - | 11 |

* Assumed value for the present analysis

## 8. FINITE ELEMENT DISCRETIZATION

The finite element discretization adopted in the present analysis is shown in Fig. 5. The entire domain (200m × 200m × 375m) has been divided into 2400, 8-noded 3-D brick elements with a total of 2752 nodes. Twenty seven stages of excavation have been simulated to excavate the cavern in 9 sections. Each section, with a length of 25 m, has been simulated in three stages of excavation (Fig. 1). Accordingly, the excavated cavern has been subdivided into 63 elements. In order to simulate the upper stage of excavation of each section, 8 elements from two layers have been removed (deactivated). Subsequently, three layers consisting of 12 elements have been removed (deactivated) as a middle stage excavation. Lower two layers consisting of 8 elements have been removed (deactivated) as the third and final stage of excavation. This sequence of material removal has been followed systematically for all the excavated sections.

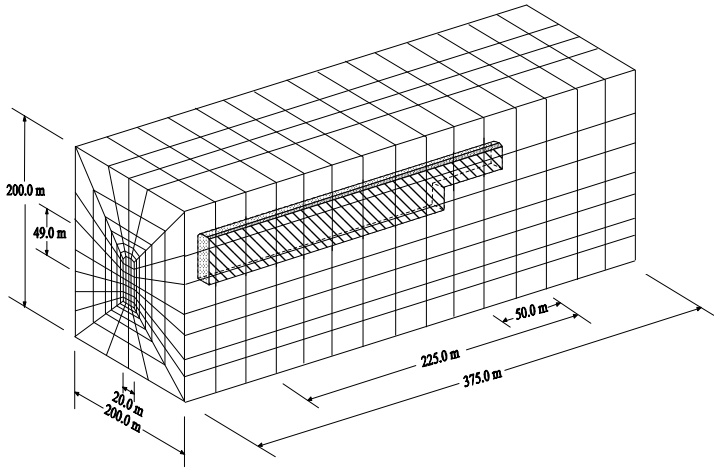


Fig. 5 - 3D-Finite element mesh adopted in present study

## 9. BOUNDARY CONDITIONS

The outer vertical boundaries of the mesh have been restrained laterally. The bottom boundary has been restrained against any vertical movement. At any stage of excavation, deactivated nodes located in the excavated area have been fully restrained with fixity condition in X, Y and Z directions.

## 10. DISCUSSION OF RESULTS

### 10.1 Deformation Pattern

#### (a) Linear analysis

The displacements of the cavern in the form of contours, as obtained from linear analysis, have been presented in Figs. 6a, b, c for only half of the cross-section owing to

symmetry in the pattern. Values of maximum displacements around the periphery of cavern have also been presented in Table 3. The contours of horizontal displacement in *x*-direction, $\delta_x$ (Fig. 6a) indicate a concentration of displacement in the sidewalls of the cavern. It may be seen from Table 3 that the maximum horizontal displacement, $\delta_x$ is of the order of 46.7mm in the sidewalls. At the crown and invert of the cavern, horizontal displacement, $\delta_x$ is of the order of 9mm and 6.7mm respectively. Figure 6b shows the contours of horizontal displacement in *y*-direction, $\delta_y$. Higher values have been observed at the crown and invert of the cavern and are of the order of 6mm and 7mm respectively. The displacements are concentrated at the upper and lower corners of the cavern. Figure 6c, which shows the vertical displacement, $\delta_z$ contours, indicates zero vertical displacement at about the mid height of cavern. Maximum values of 31.8mm (downward) and 37.1mm (upward) have been observed at the crown and invert respectively, while in the sidewall, the maximum vertical displacement is 12.8mm.

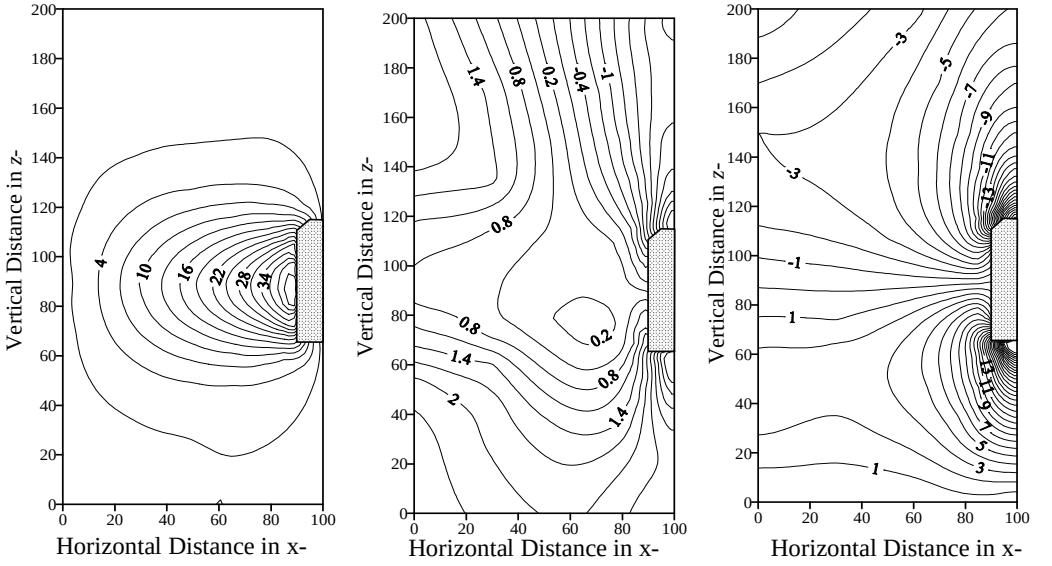


(a) Horizontal displacement ($\delta_x$) (b) Horizontal displacement ($\delta_y$) (c) Vertical Displacement ($\delta_z$)

Fig. 6 - Contours of displacement (mm) from linear stress analysis

**(b) Nonlinear analysis**

Figure 7 shows contours of horizontal displacement, $\delta_x$ typically for stage-6, stage-15 and stage-27 of the excavation. It is clear from the nature of contours that the cavern experiences higher displacements in the sidewalls which have been found to increase as the excavation proceeds. It may be seen from Table 3 that displacements around the periphery of cavern have increased considerably after the completion of section-2 (stage-6). The horizontal displacement, $\delta_x$ increases due to nonlinearity by 4.5 times and 3.3 times at the crown and at the invert of section respectively, whereas increase in the sidewalls is by 5.7 times as compared to those from the linear analysis. Increase in displacements is marginal after excavation of section-2. With the completion of excavation of cavern, final displacements are respectively 1.3 and 1.1 times the displacements of section-2 at crown and the invert, whereas displacements in the sidewalls are about 1.1 times their values after excavation of section-2. Maximum

horizontal displacement of about 40.8mm has been found in the sidewall. A similar pattern has been observed in all the stages of the excavation.

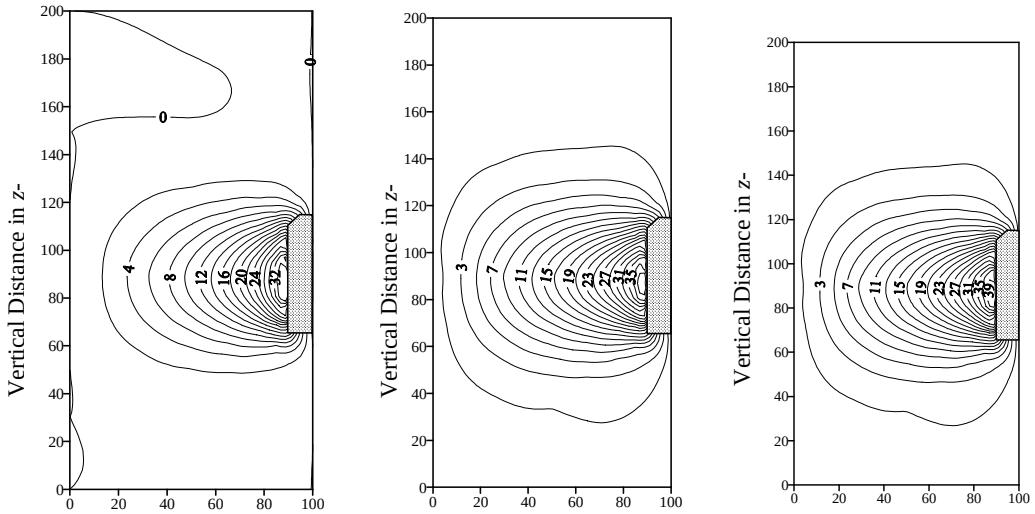


(a) Excavation Stage-6 (b) Excavation Stage- 15 (c) Excavation Stage-27

Fig. 7 - Contours of horizontal displacement, $\delta_x$ ( mm ) with stages of excavation

Table 3 - Maximum displacement at periphery of cavern from linear and nonlinear analyses

| Location | Type of Displacement | Maximum Displacement ( mm ) | | | | | | | | | |
|---|---|---|---|---|---|---|---|---|---|---|---|
| | | Linear | Nonlinear | | | | | | | | |
| | | | Section Number | | | | | | | | |
| | | | 1 | 2 | 3 | 4 | 5 | 6 | 7 | 8 | 9 |
| Crown | $\delta_x$ | ± 9.0 | ± 1.7 | ± 7.7 | ± 8.4 | 9.8 | 10.0 | 10.2 | 10.2 | 10.3 | 10.3 |
| | $\delta_y$ | -6.0 | 3.6 | -5.9 | -6.2 | -6.2 | -6.1 | -6.3 | -5.6 | -6.4 | -6.3 |
| | $\delta_z$ | -31.8 | -6.4 | -26.4 | -29.6 | -31.7 | -33.0 | -34.2 | -34.4 | -35.4 | -35.3 |
| Left Sidewa | $\delta_x$ | 46.6 | 6.6 | 37.8 | 38.0 | 38.6 | 38.6 | 39.7 | -40.5 | 40.8 | 40.8 |
| | $\delta_y$ | 5.1 | -4.7 | -3.0 | -4.0 | -4.5 | -4.9 | -5.2 | -4.5 | -5.1 | -5.0 |
| | $\delta_z$ | 12.8 | 3.7 | ± 4.9 | -8.3 | -9.3 | -10.9 | -11.5 | -12.0 | -12.4 | -12.4 |
| Right Sidew | $\delta_x$ | -46.8 | -6.6 | -37.9 | -37.9 | -38.5 | -38.5 | -39.7 | -40.6 | -40.8 | -40.8 |
| | $\delta_y$ | 5.1 | -4.7 | -3.1 | -5.1 | 12.9 | -6.1 | -4.0 | -6.5 | -6.4 | -6.2 |
| | $\delta_z$ | 12.5 | -3.6 | -5.8 | -9.3 | -10.0 | -10.7 | -11.3 | -12.0 | -12.3 | -12.2 |
| Invert | $\delta_x$ | ± 6.7 | ± 1.4 | ± 5.5 | ± 5.6 | ± 5.7 | ± 5.1 | ± 6.0 | ± 6.1 | ± 6.2 | ± 6.2 |
| | $\delta_y$ | 7.0 | 6.3 | 5.8 | 5.7 | -5.1 | -4.7 | -4.6 | -4.3 | 4.6 | 4.9 |
| | $\delta_z$ | 37.1 | 10.7 | 29.6 | 30.0 | 30.0 | 26.5 | 30.4 | 30.3 | 30.3 | 30.7 |

*Notation:* $\delta_x$ - horizontal displacement in x-direction; $\delta_y$ - horizontal displacement in y-direction; and $\delta_z$ - vertical displacement in z-direction.

The values of horizontal displacement, $\delta_y$ have shown minor changes with the progress of excavation process as is obvious in Fig. 8. A glance at Table 3 shows occurrence of a maximum horizontal displacement, $\delta_y$ of about 6.3mm and 4.9mm at the crown and invert respectively. Some change in the pattern has also been noticed during the excavation process. Generally, the displacement, $\delta_y$ is higher at the upper and lower corners of the cavern.

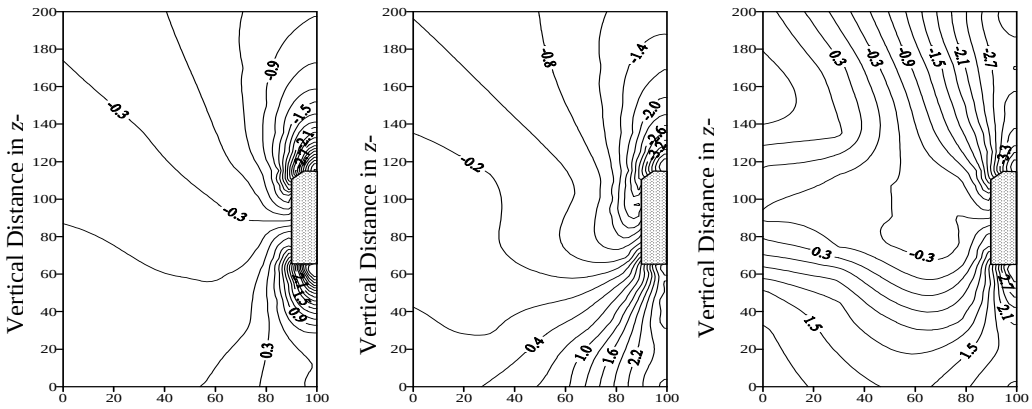


(a) Excavation Stage-6 (b) Excavation Stage-15 (c) Excavation Stage-27

Fig. 8 - Contours of horizontal displacement, $\delta_y$ ( mm ) with stages of excavation from nonlinear analysis

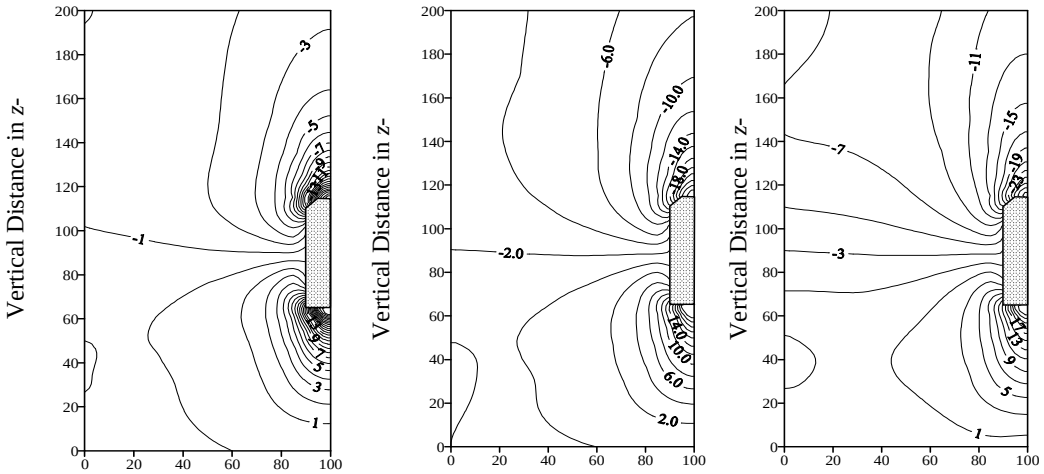


(a) Excavation Stage-6 (b) Excavation Stage-15 (c) Excavation Stage-27

Fig. 9 - Contours of Vertical Displacement, $\delta_z$ ( mm ) with Stages of Excavation from Nonlinear analysis

Changes in vertical displacement, $\delta_z$ with the progress of excavation for stages-6, 15 and 27 have been presented in Fig. 9. Analogous pattern has been observed for all the three

excavation stages. However, it may be noted from Table 3 that a sudden increase in the vertical displacement has been found at section-2 (stage-6). It shows an increase by 4.1, 1.3, 1.6 and 2.8 times at the crown, left sidewall, right sidewall and the invert respectively. Subsequent excavations have led to a reduction in the rate of increase of vertical displacement, which increases to about 1.3 times at the crown and almost no changes were found at the invert after the completion of the excavation. The vertical displacement increases in the left and right sidewalls by about 2.5 and 2.1 times respectively after the completion of the excavation process. It is clear that sidewalls undergo larger displacements as compared to those in the crown or in the invert of the cavern. This may be attributed to the high ratio of the cavern height to its width which is 2.45.

Displacement contours at the end of excavation process have been plotted along the longitudinal axis of cavern in Figs. 10 to 12. Figure 10 shows a concentration of horizontal displacements, $\delta_x$ in the region between sections-2 & 4 at the crown of the cavern. However, higher concentration of horizontal displacement, $\delta_y$ has been observed at the cavern face as depicted in Fig. 11. On the other hand, Fig. 12 shows concentration of vertical displacement, $\delta_z$ all along the crown and invert regions of the cavern. In general, displacement in the roof portion has been found to be higher than the heave at the invert of the cavern.

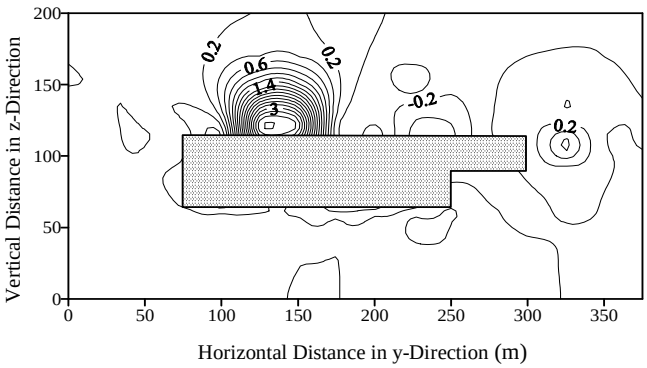


Fig. 10 - Horizontal displacement, $\delta_x$ (mm) along longitudinal axis (Centre Plane) after full excavation from nonlinear analysis

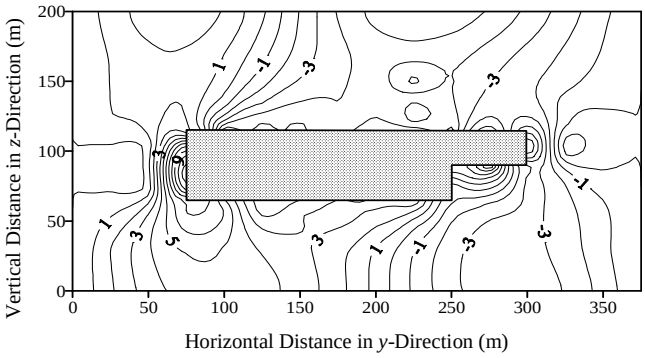


Fig. 11 - Horizontal displacement, $\delta_y$ ( mm ) along longitudinal axis (Centre Plane) after full excavation from nonlinear analysis

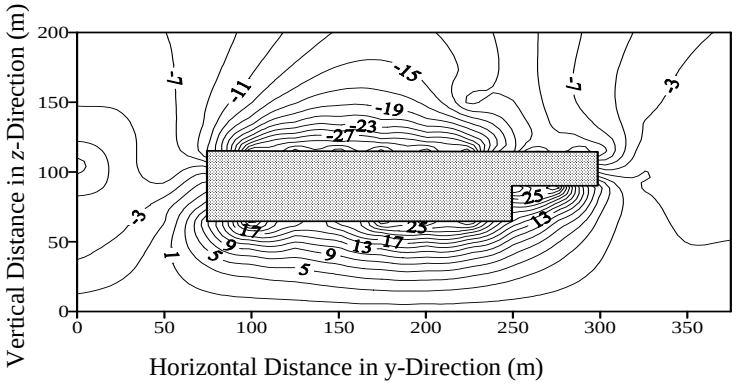


Fig. 12 - Vertical displacement, $\delta_z$ ( mm ) along longitudinal axis (Centre Plane) after full excavation from nonlinear analysis

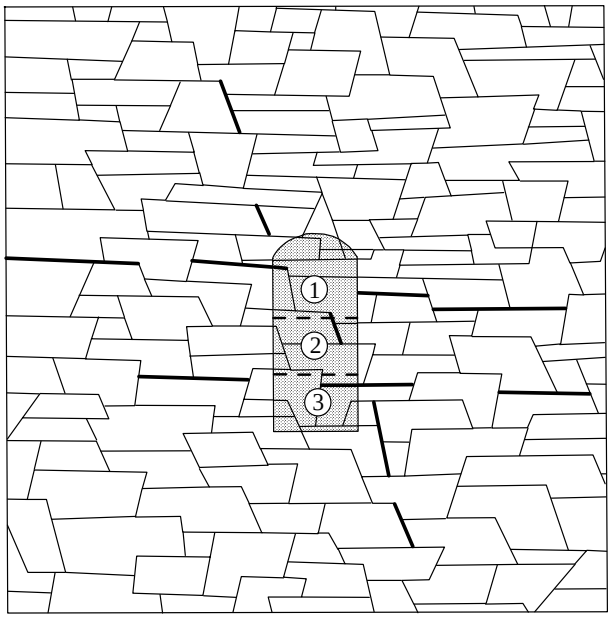


Fig. 13 - Joint pattern adopted in discontinuum analysis (Bhasin et al., 1996)

**(c) Comparison**

An attempt has been made to compare the displacements obtained from linear and nonlinear analyses. Displacements obtained from nonlinear analysis have been found to be higher than those obtained from linear analysis in the crown region. However, in the sidewalls and the invert, these have been found to be on somewhat on the lower side.

In order to verify the results obtained from the present study, comparison has also been made with the studies conducted by other research workers and also with the data procured from field instrumentation. Bhasin et al. (1996) have analyzed the cavern using a 2D-discontinuum approach using Universal Distinct Element Code (UDEC) for

the joint pattern around the cavern as shown in Fig. 13. The vertical displacement at the crown obtained by Bhasin et al. (1996) was 17.0mm which is much lower than the corresponding value of 30.7mm obtained in the present study. Figure 14 shows the contours of horizontal displacement for the case of full cavern excavation obtained by Bhasin et al. (1996) which gives the horizontal displacement of the order of 45 mm and 32 mm respectively, in the left and right sidewalls. However, the present study gives the corresponding displacement of 40 mm in both the sidewalls. The higher value of roof displacement estimated from the present study may be due to the difference in joint orientation adopted or due to the assumption regarding the joint properties, especially the stiffnesses.

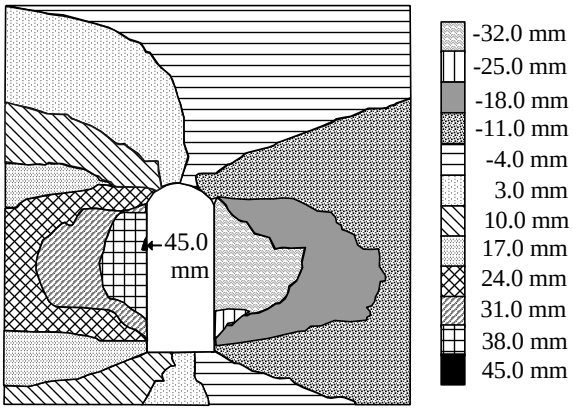


Fig. 14 - Horizontal displacement, $\delta_x$ (mm) contours from 2-D analysis (Bhasin et al., 1996)

A comparison has also been made with the results obtained by Sitharam and Latha (2002) who have used 2D-finite difference program (FLAC) with excavation sequence shown in Fig. 4. Results of their numerical experimentation along with the measured values in the field are presented in Table 4. A good agreement has been obtained for the sidewalls whereas the results do not match for the roof portion of the cavern. However, Bhasin et al. (1996) have mentioned that a displacement of about 8 mm was observed in the roof after 40 days of installation in instrument at A and 7mm in instrument at B. These values increase to 24mm and 23mm after a period of 120 days of installation. It may be noted that actual displacements should be more than the observed ones simply due to the fact that there is normally a considerable time lag between excavation and the installation of instruments. It is believed that results of the present study should be on the higher side than those recorded by the instruments. Due to the differences in assumptions as well as due to the time of installation of instruments in the field, these differences are not unexpected.

### 10.2 Stress Pattern

#### (a) Linear analysis

The contours of horizontal stress, $\sigma_x$ distribution, presented in Fig. 15a, shows the expected stress concentration near the lower edge of the cavern. The horizontal stress,

$\sigma_x$ at the crown and invert of the cavern is of the order of 9.278 MPa and 9.597 MPa respectively and reported in Table 5. Minimum horizontal stress, $\sigma_x$ has been observed in the middle of the sidewalls and it increases towards the domain boundary till it equals the in-situ stress which is about 4.8 MPa.

Table 4 - Measured and predicted deformations for Nathpa-Jhakri powerhouse cavern (Sitharam and Latha, 2002)

| Stage | Excavation Level | | Location of MPBX at EL (m) | Deformation along the Line (mm) | |
|---|---|---|---|---|---|
| | From EL (m) | To EL(m) | | Measured Values | Predicted Values |
| 1 | 1024 | 1018 | 1024 (A) | 13 – 18 | 10.0 – 14.0 |
| 2 | 1024 | 1018 | 1022 (B) | 6 – 12 | 8.2 – 13.5 |
| 3 | 1018 | 1006 | 1022 (B) | -1.3 – 2.5 | 1.0 – 2.3 |
| 4 | 1006 | 1000 | 1018 (C) | 1 – 4 | 1.4 – 3.7 |
| 5 | 1000 | 975 | 1006 (D) | 10 – 45 | 13.0 – 42.2 |
| 6 | 983 | 975 | 996 (E) | 1 - 3 | 1.3 – 4.2 |

Table 5 - Maximum average stresses at periphery of cavern from linear and nonlinear analyses

| Location | Type of Stresses | Maximum Average Stresses ( MPa ) | | | | | | | | | |
|---|---|---|---|---|---|---|---|---|---|---|---|
| | | Linear | Nonlinear | | | | | | | | |
| | | | Section Number | | | | | | | | |
| | | | 1 | 2 | 3 | 4 | 5 | 6 | 7 | 8 | 9 |
| Crown | $\sigma_x$ | -9.278 | -5.641 | -7.277 | -8.678 | -9.038 | -9.323 | -9.381 | -9.400 | -11.62 | -9.431 |
| | $\sigma_y$ | -5.094 | -5.736 | -3.609 | -3.846 | -3.829 | -3.856 | -3.879 | -3.890 | -4.962 | -4.836 |
| | $\sigma_z$ | -7.385 | -5.872 | -3.593 | -4.194 | -4.185 | -4.212 | -4.226 | -4.234 | -8.241 | -7.318 |
| Left Side wall | $\sigma_x$ | -2.859 | -5.055 | -2.940 | -2.502 | -2.442 | -2.911 | -2.826 | -2.752 | -2.782 | -3.290 |
| | $\sigma_y$ | -6.691 | -7.686 | -6.487 | -7.078 | -7.205 | -7.267 | -7.316 | -7.336 | -7.188 | -7.473 |
| | $\sigma_z$ | -10.73 | -10.47 | -10.09 | -10.65 | -11.28 | -11.60 | -11.75 | -11.90 | -10.79 | -11.91 |
| Right Side wall | $\sigma_x$ | -4.676 | -5.078 | -4.943 | -4.638 | -4.666 | -4.682 | -4.687 | -4.689 | -3.850 | -4.686 |
| | $\sigma_y$ | -6.620 | -7.663 | -6.491 | -6.926 | -7.107 | -7.166 | -7.168 | -7.287 | -7.800 | -7.481 |
| | $\sigma_z$ | -10.56 | -10.36 | -9.947 | -10.50 | -11.25 | -11.57 | -11.70 | -11.85 | -12.16 | -11.87 |
| Invert | $\sigma_x$ | -9.597 | -6.571 | -7.835 | -8.939 | -9.422 | -9.760 | -9.793 | -9.802 | -9.477 | -9.826 |
| | $\sigma_y$ | -4.144 | -6.746 | -3.973 | -3.806 | -4.332 | -4.323 | -4.281 | -4.609 | -4.108 | -4.148 |
| | $\sigma_z$ | -3.722 | -6.808 | -3.677 | -4.413 | -4.337 | -4.348 | -4.341 | -4.340 | -3.725 | -3.819 |

Notation: *$\sigma_x$: horizontal stress in x-direction, $\sigma_y$: horizontal stress in y-direction, $\sigma_z$: vertical stress in z-direction.*

Horizontal stress in *y*-direction, $\sigma_y$ has been found to be high on the periphery of the cavern as may be seen from Fig. 15b. Maximum values of about 5.094 MPa, 6.691 MPa and 4.144 MPa have been found at crown, sidewalls and invert of the cavern respectively (Table 5). These reduce away from the cavern boundary and equal to about 4.8 MPa near the domain boundary which is the in-situ stress.

Figure 15c shows a high concentration of vertical stress at the corner of the cavern. The maximum vertical stress of about 10.73 MPa has been found in the sidewalls and about 7.385 MPa and 3.722 MPa at the crown and invert of the cavern respectively. In general, most of the stresses are compressive in nature.

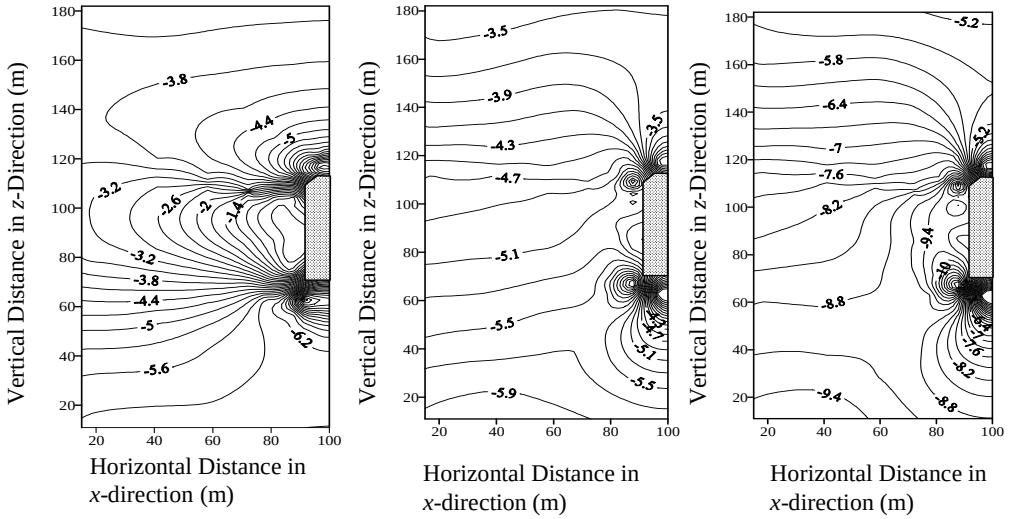


(a) Horizontal Stress ( $\sigma_x$ ) (b) Horizontal Stress ( $\sigma_y$ ) (c) Vertical Stress ( $\sigma_z$ )

Fig. 15 - Contours of average stresses ( MPa ) from linear analysis

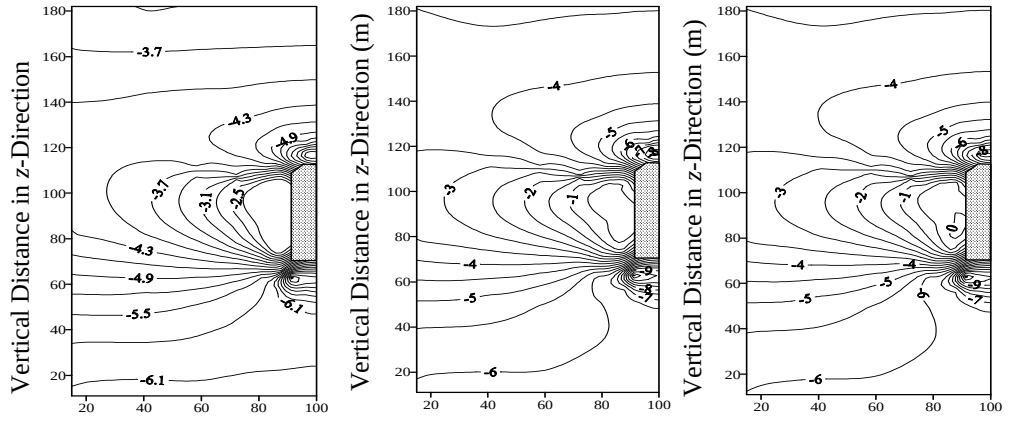


(a) Excavation Stage-6 (b) Excavation Stage-15 (c) Excavation Stage-27

Fig. 16 - Contours of average horizontal stress, $\sigma_x$ (MPa) with stages of excavation from nonlinear analysis

**(b) Nonlinear analysis**

The contours of horizontal stress, $\sigma_x$ obtained from nonlinear analysis for stage-6, stage-15 and stage-27 have been presented in Fig. 16. $\sigma_x$ increases at the crown and invert of the cavern with the stages of the excavation. It has increased by about 1.2 and 1.5 times at the crown and invert respectively when excavation proceeds from stage-1 to final stage-27 (Table 5). However, it has been found to reduce by about 1.5 times in the sidewalls. In the middle portion of the sidewalls, $\sigma_x$ has reduced to zero and increases away towards the cavern boundary till it becomes equal to the in-situ stress of 4.8 MPa.

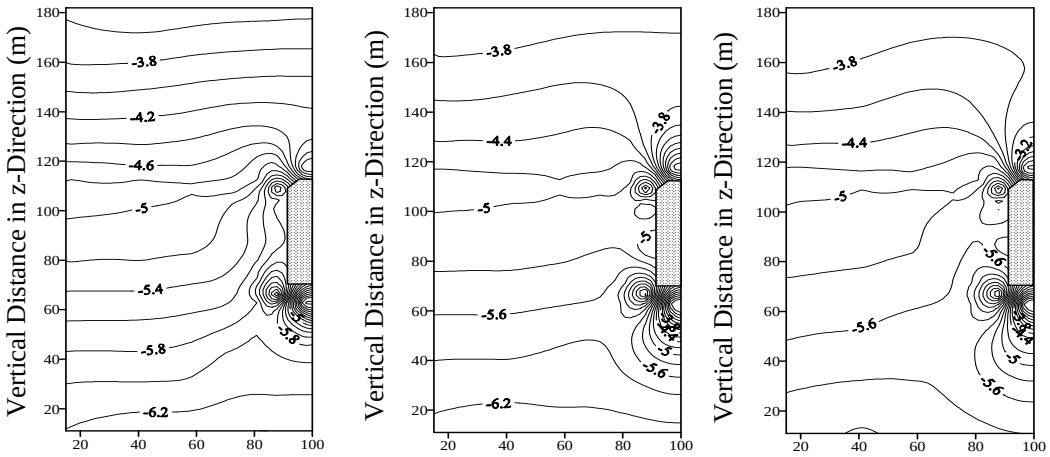


Fig. 17 - Contours of average aorizontal stress, $\sigma_y$ ( MPa ) with stages of excavation from nonlinear analysis

Minor changes have been obtained in the horizontal stresses, $\sigma_y$ due to the excavation process as shown in Fig. 17 and Table 5. The stresses have been found to be concentrated at the corner of the cavern. A maximum value of 7.0 MPa was found in the sidewalls. As seen in Table 5, the maximum value of $\sigma_y$ at the crown and at the invert has reduced from 5.736 MPa to 5.094 MPa and from 6.746 MPa to 4.144 MPa respectively as the excavation progress from section-1 to section -9 in the final stage of excavation.

In general, the vertical stress, $\sigma_z$ shows an increasing trend as excavation proceeds as shown in Fig. 18. It may be noted from Table 5 that the maximum value of $\sigma_z$ has increased from 5.872 MPa (stage-3) to 7.318 MPa (stage-27) in the crown, from 10.477 MPa (stage-3) to 11.138 MPa (stage-27) in left-sidewall and from 10.363 MPa (stage-3) to 11.868 MPa (stage-27) in the right-sidewall. The invert of the cavern shows an exception when the vertical stress reduces by 1.8 times after full excavation (stage-27) compared to the value of $\sigma_z$ at the end of stage-3 of excavation. A maximum compressive stress of the order of 17.5 MPa has been observed near the corner. Away

from the boundary of the cavern, the vertical stress has been found to decrease till it finally equals the in-situ stress. All vertical stresses are compressive in nature.

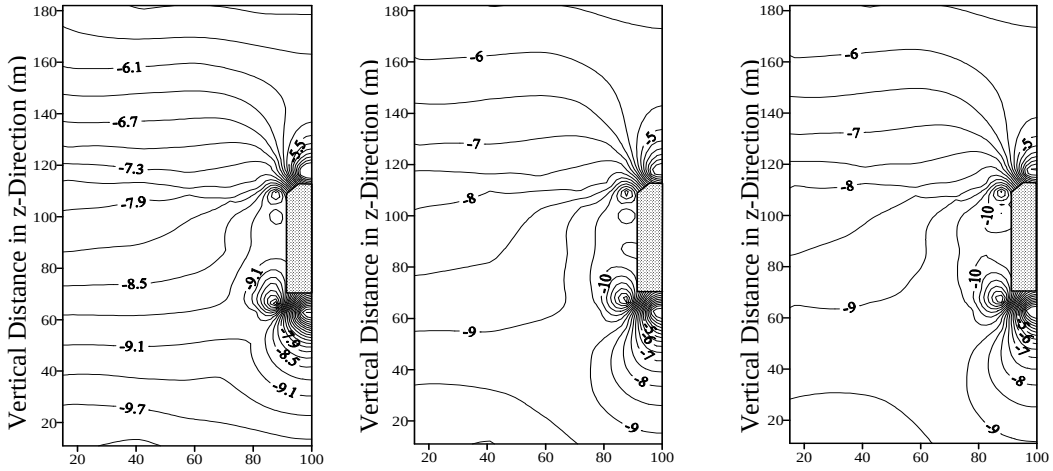


Fig. 18 - Contours of average vertical stress, $\sigma_z$ ( MPa ) with stages of excavation from nonlinear analysis

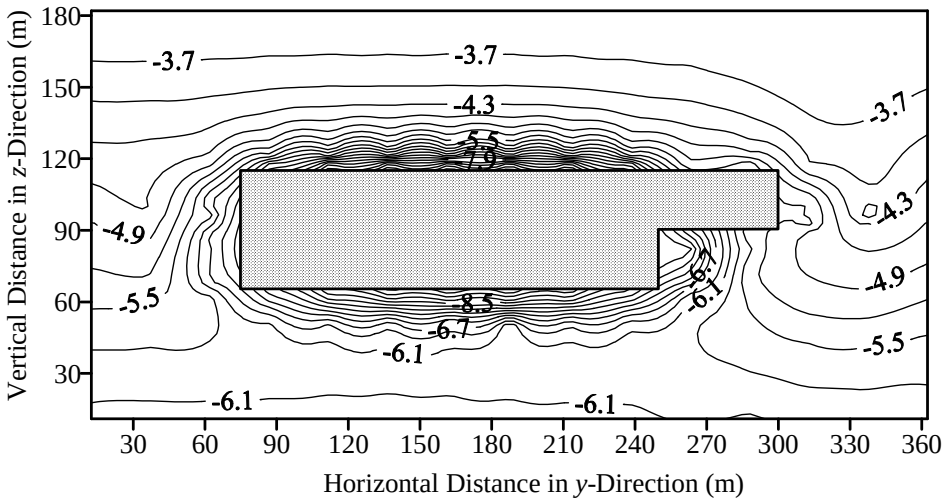


Fig. 19 - Average horizontal stress, $\sigma_x$ ( MPa ) along longitudinal axis (Centre Plane) from nonlinear analysis

Figures 19, 20 and 21 show the distribution of the stresses $\sigma_x$, $\sigma_y$ and $\sigma_z$ respectively along the longitudinal axis of the cavern. The horizontal stress, $\sigma_x$ is more at the cavern periphery (Fig. 19), whereas $\sigma_y$ is on the lower side (Fig. 20). Figure 21 shows a reduction in vertical stress near the periphery of cavern at the locations of crown and invert.

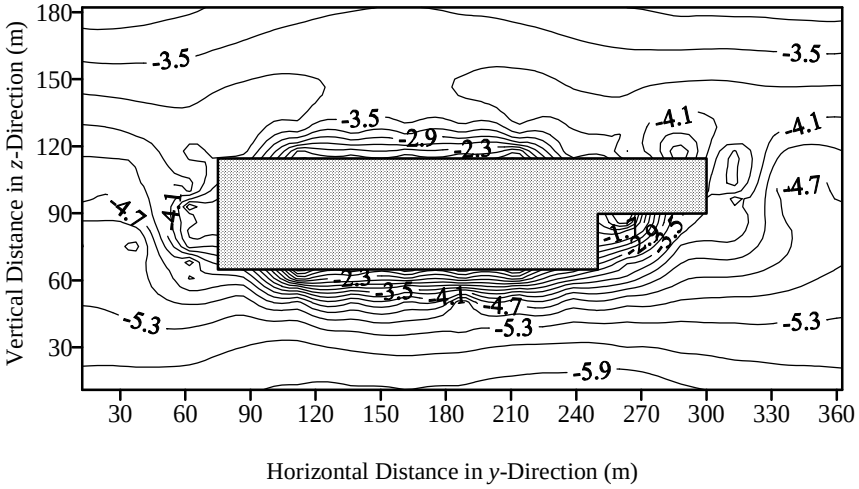


Fig. 20 - Average horizontal stress, $\sigma_y$ ( MPa ) along longitudinal axis (Centre Plane) from nonlinear analysis

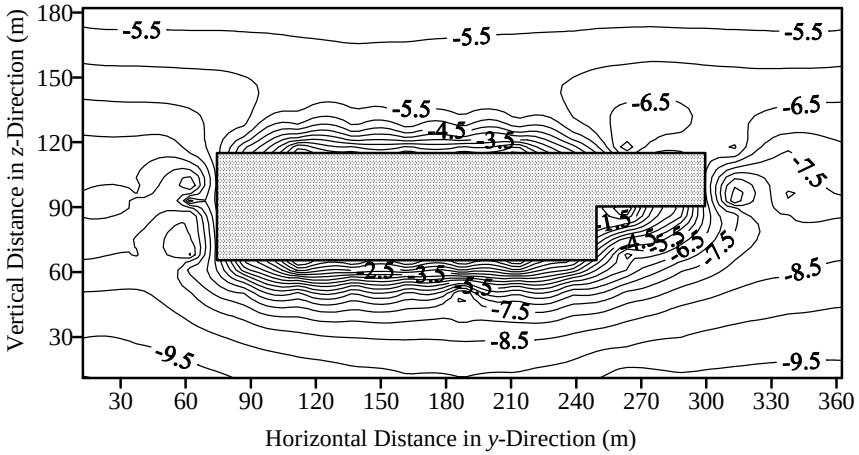


Fig. 21 - Average vertical stress, $\sigma_z$ ( MPa ) along longitudinal axis (Centre Plane) from nonlinear analysis

### (c) Comparison

In general, it may be concluded that the average stresses from linear analysis are insignificantly higher than those obtained from nonlinear analysis.

## 10.3 Principal Stress Pattern

### (a) Linear analysis

Figure 22 shows the distribution of the average principal stresses around the periphery of the cavern. In general, higher stress concentration has been found around the corners of the cavern. All the stresses are compressive in nature. Average minor principal stress,

$\sigma_3$ decreases away from the cavern periphery and is negligible at the mid height of the sidewalls (Fig. 22a). However, Fig. 22b shows almost no variation in intermediate principal stress, $\sigma_2$ at any specified section. The principal stresses are about the same order of magnitude as in-situ stresses of 4.8 MPa far away from the excavated boundary. The major principal stress, $\sigma_1$ is maximum along the periphery and reduces to the in-situ stress of 7.74 MPa (Fig. 22c) away from the excavation boundary.

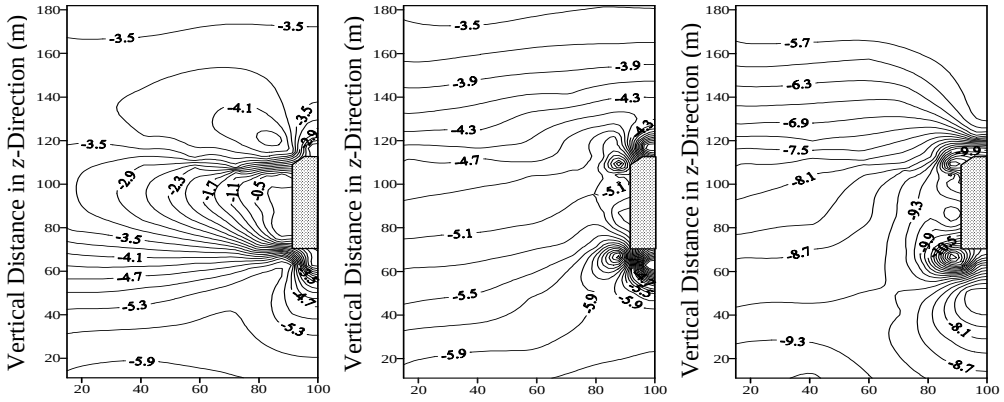


(a) Minor Principal Stress ( $\sigma_3$ ) (b) Intermediate Principal Stress ( $\sigma_2$ ) (c) Major Principal Stress ( $\sigma_1$ )

Fig. 22 - Contours of average principal stresses (MPa) from linear analysis

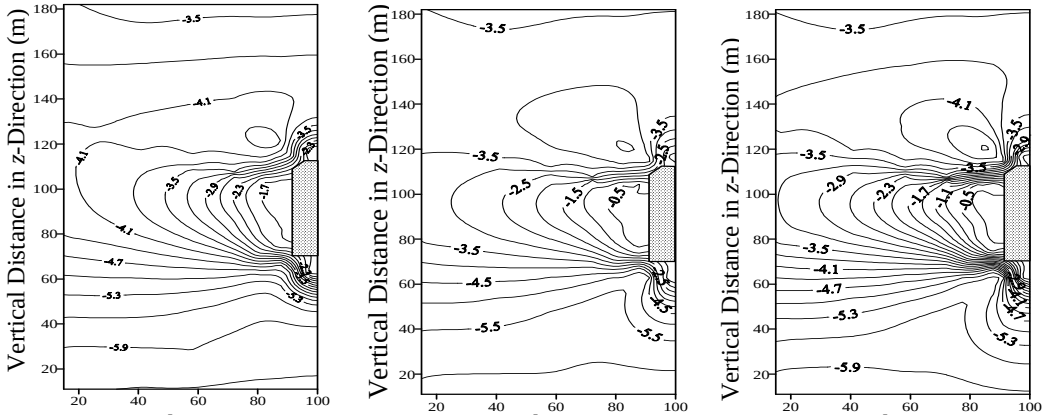


(a) Excavation Stage-6 (b) Excavation Stage-15 (c) Excavation Stage-27

Fig. 23 - Contours of average minor principal stress, $\sigma_3$ ( MPa ) with stages of excavation from nonlinear analysis

**(b) Nonlinear analysis**

The contours of minor and intermediate principal stresses for stage-6, stage-15 and stage-27 of excavation have been presented in Figs. 23 and 24 respectively. The stresses

are concentrated near the periphery of the cavern. Similar behavior was also observed in linear analysis. Figure 25 shows the variation of major principal stress around the cavern. All the stresses are compressive in nature. Higher concentration of the major principal stress has been found in the sidewalls of the cavern. A maximum compressive stress of the order of 19 MPa has been obtained near the lower corner of the cavern.

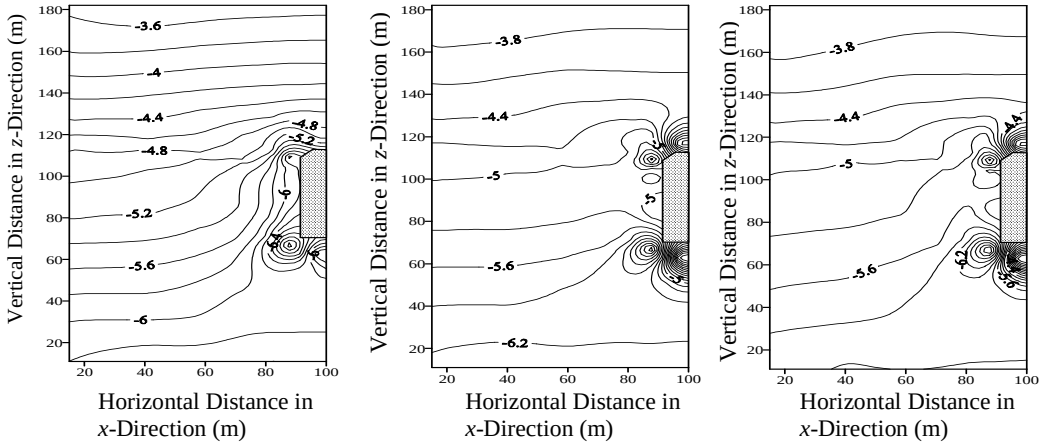


Fig. 24 - Contours of average intermediate principal stress, $\sigma_2$ ( MPa ) with stages of excavation from nonlinear analysis

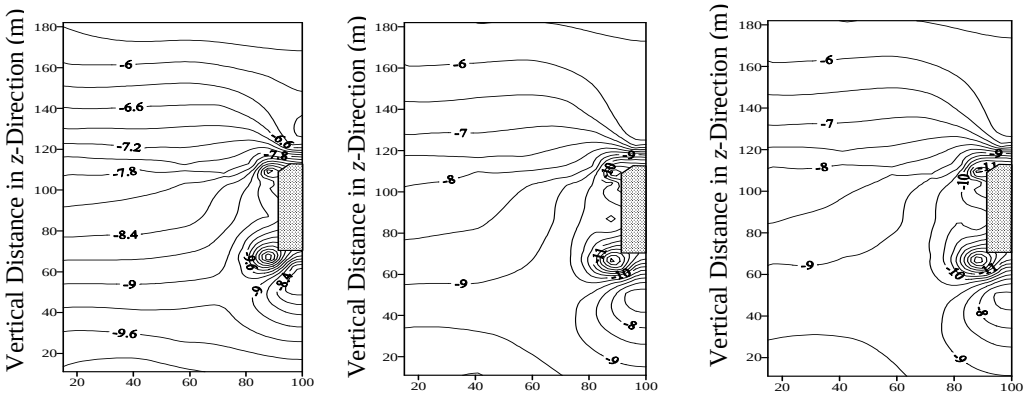


Fig. 25 - Contours of average major principal stress, $\sigma_1$ ( MPa ) with stages of excavation from nonlinear analysis

### (c) Comparison

The stresses obtained from Bhasin et al. (1996) and those obtained from the present study after the final stage of the excavation have been compared. Bhasin et al. (1996), using a 2D-discontinuum approach and joint pattern shown in Fig. 13, have reported maximum principal stresses of about 9.0 MPa, 25.0 MPa and 21.0 MPa in the crown,

left-sidewall and right-sidewall respectively. The corresponding values obtained from the nonlinear analysis in the present study are 13.31 MPa, 18.62 MPa and 19.2 MPa respectively. The higher values in the crown obtained in the present study may be due to the flat shape of the roof adopted in the present study which attracts a higher stress concentration. However, Bhasin and his co-workers (Bhasin et al., 1996) considered the roof as concave which causes a lesser stress concentration.

The difference in the behavior obtained from different studies is expected especially when different assumptions have been made in each study. Another significant reason may be the values of stiffnesses of the joints which have been assumed in the present analyses.

## 11. CONCLUSIONS

On the basis of linear and nonlinear analyses of Nathpa Jhakri hydropower project and comparison of results with the field observed behavior, it has been found that -

(i) The methodology proposed by Sharma et al. (2001) for 2-D simulation of sequence of excavation has been modified in the present study for dealing with 3-D situations.
(ii) The displacements obtained from linear analysis, considering single stage excavation are, in general, higher than those obtained from nonlinear analysis considering the sequence of excavation.
(iii) The displacements obtained from nonlinear analysis compare reasonably well with the measured displacements as well as those obtained from other numerical analyses.
(iv) The stresses obtained in present study from 3-D analysis considering the sequence of excavation are lower than those obtained by other research workers from 2-D analyses.
(v) 3-D analysis is more appropriate for large underground structures in jointed media having different attitude of joints. Results obtained in the present study prove the capability of the software package developed for analyzing the stability of underground structures excavated in varying and complex geological settings.
(vi) Results obtained in present study show that the excavation of section-2 (stage-6) is the most critical section. It is not essential that the final stage of excavation proves to be critical from stability point of view. The present study has shown that instability may occur at any intermediate stage of excavation.
(vii) Comparison of results has proved the efficiency of the constitutive laws proposed herein to simulate the nonlinearity of jointed rock mass.
(viii) The type and the number of stages selected for simulation of excavation significantly influence the redistribution of stresses and, in turn, the stability of underground structures.
(ix) Using present 3-D simulation of excavation process, it may be possible to assign a critical stage of excavation in the excavation of such large size caverns in jointed rock masses and therefore a perfect scheme of excavation from view of safety and economy can be decided a-priori.

***References***

Bandis, S. C., Lumsden, A. C. and Barton, N. R. (1983). Fundamentals of Rock Joint Deformation, *Int. J. Rock Mech. Min. Sci. & Geomech. Abst.*, Vol. 20, No. 6, pp. 249-268.

Bhasin, R. K., Barton, N., Grimstad, E., Chryssanthakis, P. and Shende, F. P. (1996). Comparison of Predicted and Measured Performance of a Large Cavern in the Himalayas, *Int. J. Rock Mech. Min. Sci. & Geomech. Abst.*, Vol. 33, No. 1, pp. 607-626.

Bhasin, R., Barton, N., Grimstad, E. and Chryssanthakis, P. (1995). Engineering Geological Characterization of Low Strength Anisotropic Rocks in the Himalayan Region for Assessment of Tunnel Support, *Engng. Geol.*, Vol. 40, No. 1/2, pp. 169-193.

Borja, R. I., Lee, S. R. and Seed, R. B. (1989). Numerical Simulation of Excavation in Elastoplastic Soils, *Int. J. Num. & Analy. Meth. in Geomech.*, Vol. 13, No. 3, pp. 231-249.

Chauhan, R. S. (1999). Excavation and Support Measures of Desilting Chambers of Nathpa Jhakri Project, *Seminar on Rock Mech. and Tunnelling Tech. (with Special Reference To NJPC Hydroelectric Power Project), ISRMTT*, New Delhi (India), pp. 71-80.

Chryssanthakis, P., Bhasin, R., Barton, N. (1996). Using NMT Principles in Predicting Performance of a Power-House in the Himalayas, India, *Conf. on Recent Advances in Tunnelling Tech.*, Vol. I, New Delhi (India), pp. 143-155.

Clough, G. W. and Mana, A. I. (1976). Lessons Learned in Finite Element Analysis of Temporary Excavations, *2nd Int. Conf. on Num. Meth. in Geomech.*, Vol. 1, Blacksburg, VA (US), pp. 496-510.

Christian, J. T. and Wong, I. H. (1973). Errors in Simulation of Excavation in Elastic Media by Finite Elements, *Soils & Foundations*, Vol. 13, No. 1, pp. 1-10.

Clough, R. W. and Woodward, R. J. (1967). Analysis of Embankment Stresses and Deformations, *J. Soil Mech. & Found. Div., ASCE*, Vol. 93, No. SM4, pp. 529-549.

Comodromos, E., Hatzigogos, Th. and Pitilakis, K. (1993). Multi-Stage Finite Element Algorithm for Excavation in Elasto-Plastic Soils, *Computers & Structures*, Vol. 46, No. 2, pp. 289-298.

Dasgupta, B. (1998). Use of Numerical Modelling for Underground Excavation, *National Workshop on Undergr. Space Utilisation, ISRMTT*, New Delhi (India), pp. 165-183.

Desai, C. S. and Sargand, S. (1984). Hybrid FE Procedure for Soil-Structure Interaction, *J. Geotech. Engng. Div., ASCE*, Vol. 110, No. 4, pp. 473-486.

Gupta, A. (1999). Planning and Layout of Nathpa Jhakri Project, *Seminar on Rock Mech. and Tunnelling Tech. (with Special Reference To NJPC Hydroelectric Power Project), ISRMTT*, New Delhi (India), pp. 1-12.

Mana, A. I. and Clough, C. W. (1981). Prediction of Movements for Braced Cuts in Clays, *J. Geotech. Engng. Div., ASCE*, Vol. 107, No. GT6, pp. 759-777.

Najjar, Y. and Zaman, M. (1993). Surface Subsidence Prediction by Nonlinear Finite-Element Analysis, *J. Geotech. Engng. Div., ASCE*, Vol. 119, No. 11, pp. 1790-1804.

Ranadive, M. S. and Parikh, S. K. (2003). Effect of Residual Stresses and Sequence of Excavation on Displacement of Tunnel by Finite Element Method, *Indian Geotech. J.*, Vol. 33, No. 3, pp. 291-310.

Sharma, V. K. and Chauhan, K. S. (1999). Excavation and Supporting System for Power House Cavern, *Seminar on Rock Mech. and Tunnelling Tech. (with Special Reference To NJPC Hydroelectric Power Project), ISRMTT*, New Delhi (India), pp. 95-106.

Sharma, K. G., Varadarajan, A. and Srivastava, R. K. (1985). Elasto-Viscoplastic Finite Element Analyses of Tunnels, *5th Int. Conf. Num. Meth. in Geomech.*, Vol. 2, Nagoya (Japan), pp. 1141-1148.

Sharma, K. G., Varadarajan, A. and Desai, C. S. (2001). Improved Finite Element Simulation of Excavation in Elastic and Elasto-Plastic Geologic Media, *J. Rock Mech. & Tunnelling Tech.*, Vol. 7, No. 1, pp. 11-28.

Sirkek, J. K., Negi, B. S. and Thakur, D. D. (1999). Tunnelling with Special Drilling Rig through Bad Rock, *Seminar on Rock Mech. and Tunnelling Tech. (with Special Reference To NJPC Hydroelectric Power Project), ISRMTT*, New Delhi (India), pp. 171-181.

Sitharam, T. G. and Latha G. M. (2002). Equivalent Continuum Analysis of a Large Cavern in Jointed Rock, *ISRM Regional Symp.- Advancing Rock Mech. Frontiers to Meet Challenges of 21st Century*, New Delhi (India), pp. V7-V15.

Wang, J. G., Ichikawa, Y. and Leung, C. F. (2003). A Constitutive Model for Rock Interfaces and Joints, *Int. J. Rock Mech. & Min. Sci.*, Vol. 40, No. 1, pp. 41-53.